MRS Advances

Spray-Deposited Metal-Chalcogenide Photodiodes for Low Cost Infrared Imagers

Journal:	*MRS Advances*
Manuscript ID	Draft
Manuscript Type:	Regular Article
Date Submitted by the Author:	n/a
Complete List of Authors:	Boykin II, Tommy; University of Central Florida, Physics Dhakal, Nagendra; University of Central Florida, Physics Boroumand, Javaneh; University of Central Florida, Physics Gonzalez, Francisco Javier; University of Central Florida, Department of Physics Oladeji, Isaiah; SISOM THIN FILMS LLC, Figueiredo, Pedro; University of Central Florida, Physics Neushul, Stephen; iCRco Peale, Robert; University of Central Florida, Physics
Keywords:	photovoltaic, semiconducting, optoelectronic

MRS Advances

Spray-deposited metal-chalcogenide photodiodes for low cost infrared imagers

Tommy O. Boykin II,[1,2] Nagendra Dhakal,[1,2] Javaneh Boroumand,[1] F. Javier Gonzalez,[1,2] Isaiah O. Oladeji,[2] Pedro Figueiredo,[2] Stephen Neushul,[3] and Robert E. Peale[1,2]

[1] *Physics, University of Central Florida, Orlando, FL 32816 USA*

[2] *Truventic LLC, 1209 W. Gore St. Orlando, FL 32805 USA*

[3] *iCRco, Goleta, CA*

Abstract

Low-cost, light-weight, low-power, large-format, room-temperature, mid-wave infrared (MWIR) detectors are needed for reduced-scale aircraft. An opportunity, suggested by direct-read X-radiography systems, is the use of thin film transistor (TFT) array as read-out integrated circuit (ROIC) for low-cost sensors deposited directly and unpatterned onto this ROIC. TFTs have already been thoroughly optimized for power, weight, large-format, and cost by the flat-panel-display industry. We present experimental investigation of aqueous-spray-deposited, mid-wave-IR, metal-chalcogenide heterojunction CdS/PbS photodiodes for this application. Measured responsivity, detectivity D, and photoresponse spectra are reported.*

INTRODUCTION

Low cost infrared detector technology is needed in the 1-to-2.7 and 3-to-5 μm wavelength bands. These correspond to spectral windows of high atmospheric transmission, usually referred to as short-wave (SWIR) and mid-wave (MWIR) infrared. This need was articulated by the US Air Force in a recent Small Business Innovative Research (SBIR) solicitation [1]. We describe preliminary research performed to support a proposal for that solicitation.

Current SWIR and MWIR imaging systems are expensive, power hungry, bulky, and require cryogenic operating temperatures. These factors make them poorly suited for deployment in (e.g.) unmanned aerial vehicles. An inexpensive, compact, ambient-temperature imager would enable new infrared applications.

Costs can be reduced and manufacturing throughput increased by depositing a photosensitive film directly and unpatterned on a read-out integrated circuit (ROIC). ROIC pitch should be 10-30 μm to compete with current technology. The ROIC itself should be inexpensive.

We consider the conventional thin film transistor (TFT) array as a potential ROIC. TFTs have achieved extraordinary economies of scale and optimization in the flat-panel-display industry. An inspiration for considering TFTs as an IR-detector ROIC is their established use in commercial direct-read X-ray imagers, e.g. [2]. UCF has developed a detailed fabrication process for a suitable TFT under contract from iCRco [3]. This process, comprising just 7 contact photo-masks, was designed for execution in a university wafer fab for the purpose of developing experimental X-ray imager prototypes. Figure 1 presents a schematic for a single element of the designed TFT at the final stage of processing. Interconnects that allow control of each TFT for reading the stored charge are part of this entirely conventional design.

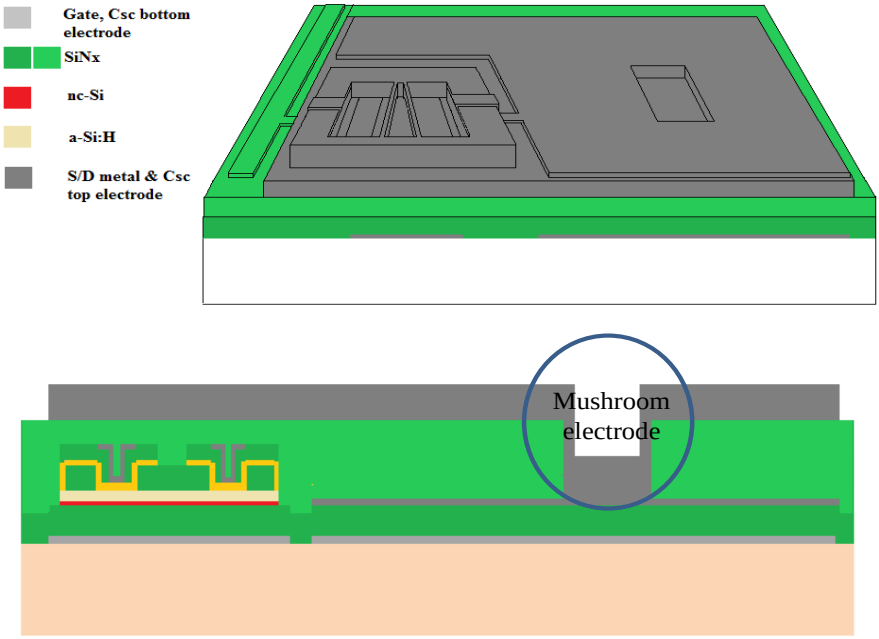

Figure 1. Structure of thin film transistor with large collection electrode.

For the TFT-based X-ray imager, an X-ray phosphor, e.g. amorphous selenium, is deposited unpatterned directly on the TFT. The material is sufficiently insulating that neighboring collection electrodes in the array are electrically isolated from each other. The top surface of the phosphor is negatively biased relative to the buried collection electrode via a thin top electrode metal. X-rays that impinge on the phosphor create electron-hole pairs. The electrons are collected by the mushroom electrode of the TFT. Subsequently, the collected charge is read out by gating the TFT connected to each collection electrode.

The TFT design of Figure 1 is based on amorphous silicon. Such TFTs have been designed with integrated amorphous-silicon bolometers to detect and image in the long-wave 8-12 μm wavelength band [4]. However, the extra processing to produce thermally-isolated air-bridge bolometers defeats the low-cost goal, and the long-wave IR is unresponsive to the articulated need [1].

Our focus is on quantum detectors that integrate an absorber with suitable MWIR bandgap. Lead-chalcogenides such as PbS and PbSe are narrow-gap semiconductors established as MWIR photoconductors [5]. We have been investigating inexpensive Pb-chalcogenide infrared photoconductors [6] and photodiodes [7]. This material can be deposited unpatterned directly onto a TFT ROIC, in principle.

If we follow the direct-read X-ray imager example and deposit a simple photoconductor such as PbS directly and unpatterned on a TFT, neighboring collection electrodes would be shorted. This is due to the excessive room-temperature conductivity of a narrow-gap semiconductor. Any collected image would be washed out before it could be read out by a TFT.

A heterojunction photodiode using a wide-gap semiconductor deposited first would isolate neighboring electrodes. IR photodiodes fabricated from n-CdS/p-PbSe heterojunctions are known [8, 9], as are CdS/PbS solar cells [7, 10, 11]. CdS is usually a window layer to allow near-IR and visible solar radiation to reach the Pb-chalcogenide absorber. By inverting this structure, an unpatterned deposition on a TFT array could sufficiently isolate the neighbouring collection electrodes. Figure 2 (left) illustrates this concept schematically. Minority-carrier electrons excited in the upper negatively biased p-type Pb-chalcogenide would be swept through the n-type CdS layer to the collection electrodes.

The purpose of this paper is to present characterization results on preliminary spray-deposited p-PbS/n-CdS heterojunction photodiodes. Though PbSe is indicated in Figure 2, we chose the similar but higher-gap PbS for initial investigation, because it is easier to deposit by our method.

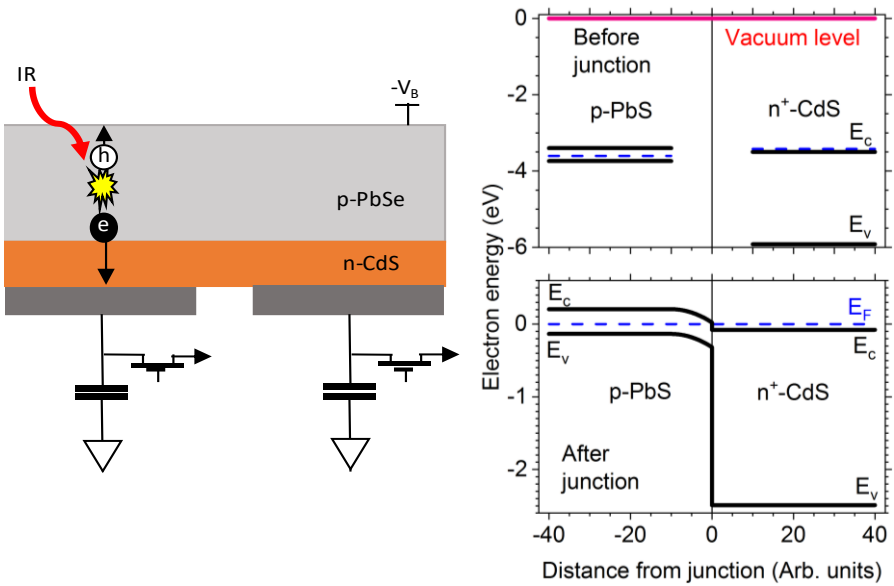

Figure 2. (left) Schematic of unpatterned infrared heterojunction photodiode deposited on TFT array. (right) Band-bending at the heterojunction constructed assuming Anderson's rule.

THEORETICAL CONSIDERATIONS

Our n-CdS films are degenerately doped, according to Hall data. Our p-PbS films are nearly intrinsic, according to the measured Seebeck coefficient S [12] and the formula [13]

$$S = (k_B/e) \ln(N_v/p) \quad (1)$$

where p is the hole concentration, k_B the Boltzmann's constant, e the electron charge, and N_v the effective density of states in the valence band [14]. From carrier concentrations, we determine the Fermi-levels indicated in Figure 2 (right, upper) using standard equations of semiconductor statistics [14].

We apply Anderson's rule [15] to establish the band-bending at the PbS/CdS heterojunction. Band positions before junction are referenced to the vacuum level, as shown in Figure 2 (right, upper). The conduction bands are positioned below the vacuum level by the electron affinity χ for each material. The value of χ_{CdS} is between 3.8 and 4.8 eV for bulk CdS [16], where the lower value corresponds to less pristine surfaces. However, a value for χ_{CdS} as low as 3.47 eV has been experimentally determined for polycrystalline chemical-bath-deposited (CBD) CdS films [11], which are closely related to those that we fabricate. This low value leads to a band diagram that best explains the experimental observations reported here. We take the value χ_{PbS} = 3.4 eV [17].

Next, the junction is formed and the bands fixed at the interface. Then, the bands in the field-free regions far from the interface are shifted vertically until the Fermi-level is constant throughout. The result is shown in Figure 2 (right, lower). This picture, with no band-bending in the CdS, is equivalent to that for a metal-semiconductor junction with the n^+-CdS playing the role of the metal. When the work function for the metal is smaller than for a p-type semiconductor, a rectifying Schottky diode is formed [14].

Applying the analysis of a metal-semiconductor Schottky diode [14] to our CdS/PbS structure, the barrier for minority-hole flow from n^+-CdS to semiconductor Φ_B is

$$\Phi_B = E_G + \chi_{PbS} - \Phi_{CdS} \quad (2)$$

where E_G is the PbS gap, and Φ_{CdS} is the CdS work function. The built-in potential V_{bi} is

$$V_{bi} = (1/q) [\Phi_B - (E_F\text{-}E_V)_{FB}] \quad (3)$$

where q is the electron charge and $(E_F\text{-}E_V)_{FB}$ is the energy separation between the PbS Fermi level and the valence band in the flat band region far from the junction. The zero-bias depletion width W in PbS is

$$W = [2 K_s \varepsilon_o V_{bi}/(q N_A)]^{1/2} \quad (4)$$

where K_s is the PbS static dielectric constant, ε_o the permittivity of free space, and N_A the acceptor concentration.

EXPERIMENTAL DETAILS

CdS/PbS photodiodes were grown on stainless steel sheets by an aqueous-spray technique called Streaming Process for Electrodeless Electrochemical Deposition (SPEED) [6]. The heterogeneous chemical reactions involved in the growth of nano-

crystalline thin films of these materials have been described in [6, 7]. Post growth anneal was done in nitrogen atmosphere.

CdS films were degenerately doped with Al. For a given x moles of Cd ions in the precursor solution, 0.1·x moles of Al were added as dopants. This translates to about 2.5 weight % of Al. Al has 3 valence electrons, while Cd has two, so Al should act like a substitutional n-type donor. Such behavior has been reported for CBD CdS [18]. Measured resistivity and carrier concentration as a function of Al doping is reported here to confirm the doping effect in SPEED-grown CdS. These quantities were evaluated by Hall measurements at room temperature in a Van der Pauw four-point probe configuration, using indium contacts, in an automated Hall effect system (Ecopia HMS-3000, Bridge Technology) with 0.55 T magnetic induction.

The Al-doped CdS layer was annealed at 450 ˚C. Then, a PbS layer was deposited and annealed at 400 ˚C. The films were diced to 6.3 mm x 6.3 mm dimensions. The current-voltage (I-V) curves were characterized at room temperature for each sample. A pressed copper contact with area slightly smaller than the sample area was used for most of these measurements. For photoresponse measurements, electrical contact was made by gold wire-bonding directly to the PbS surface.

Samples with the most diode-like I-V curves were mounted on leadless ceramic chip carriers. For photoresponse measurements, the chip carriers were mounted and exposed to infrared radiation from a blackbody radiation source with variable aperture. The blackbody radiation was modulated using a variable speed chopper. The photo-current was collected and amplified by a low-noise current amplifier (Stanford Instruments SR570) with no bias applied between the PbS surface and stainless steel substrate. The voltage output of the SR570 was synchronously amplified by a Stanford Instruments SR530 lock-in.

Responsivity was calculated from the radiance (W/m^2-sr) at the blackbody temperature in the 1-4 μm wavelength band. The band's radiance was calculated using the iPhone application bbTool. The spectral response of the diode remains unknown, though it is expected to resemble the absorption spectrum of PbS. A band with flat response from 1 to 4 μm wavelength was considered as a first approximation. This band radiance was multiplied by the blackbody aperture area (m^2) and by the solid angle subtended by the detector from the aperture (sr) to obtain the IR power incident on the detector.

For noise measurements, the photodiode dark output was amplified by a low-noise current amplifier (Stanford Instruments SR570). Amplified output was then characterized by a Hewlett-Packard 3582A Spectrum Analyzer to obtain a voltage noise spectral density $V/(Hz)^{1/2}$ near 10 kHz, which was multiplied by amplifier sensitivity (A/V) to obtain current noise spectral density. The responsivity was multiplied by the square root of the detector area and divided by the current noise spectral density to obtain the detectivity (D*).

RESULTS

Figure 3 (left) presents an SEM image of the surface of a PbS film deposited on CdS. There is structure on the length scale of ~5 μm, which may help reduce Fresnel reflection. Otherwise, the film appears smooth and without cracks.

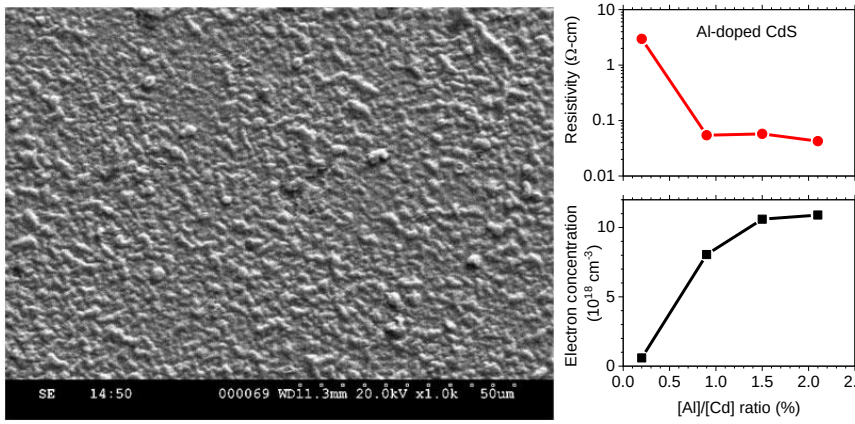

Figure 3. (left) Scanning electron microscope image of PbS surface. (right) Electrical properties of Al-doped CdS.

The conductivity type of individually deposited CdS and PbS films was confirmed by a hot probe. The voltage of the hot side was observed to be positive with respect to the cold side for CdS, which confirms n-type conductivity. The voltage of the hot side was observed to be negative with respect to the cold side for PbS, which confirms p-type conductivity. Thermoelectric effect in our PbS films has been reported in [12].

Resistivity for unannealed SPEED-grown PbS films has been reported to be 720 Ω-cm. This value reduced to 1 Ω-cm for films annealed in sulfur vapor [12]. Resistivity for SPEED-grown PbS annealed in Selenium vapor was also about 1 Ω-cm [6]. For the present work, the annealing of PbS films was done in nitrogen, so we expect the resistivity to be between 1 and ~700 Ω-cm. Hole concentrations were estimated from the published Seebeck coefficients of our films with those end point resistivities using Equation 1. We find that the high resistivity material is intrinsic, while the low resistivity material has a hole concentration of only twice the intrinsic concentration (n_i), putting the Fermi level about 20 meV below mid-gap. This is the Fermi-level position represented in Figure 2.

Figure 3 (right) presents new results for SPEED-grown Al-doped CdS. The horizontal axis values are concentration ratios of Al-salt to Cd-salt added to the precursor solutions. The ratio used for batch 3 samples was 10%, which is off scale on Figure 3 (right), but due to saturation we expect the electrical properties to resemble those at 2 %. For this electron concentration, CdS is degenerately doped, and the Fermi level lies above the conduction band minimum by 78 meV. This position was used in Figure 2.

Figure 4 (left) presents current density as a function of voltage (j-V) for one of the PbS/CdS junction samples. Two curves are plotted, one for the copper press contact and one for the gold wire-bond contact. To determine the effective area of the gold wire-bond contact, its reverse bias j-V curve was scaled to match that of the broad-area copper press contact. An effective area of 1.4 mm^2 was determined for the wire-bond, which is larger than the physical contact area. This effective area was the detector area used to calculate responsivity and D*.

Rectification is reduced for the gold wire-bond contact in comparison to the copper-PbS press contact. The rectification ratio for the copper-PbS press contact is 6.3 at applied voltages of ± 0.8 V. In comparison, the rectification ratio for the gold wire-bond contact is 1.2 at the same applied voltages. We discuss the nature of the contacts in the next section.

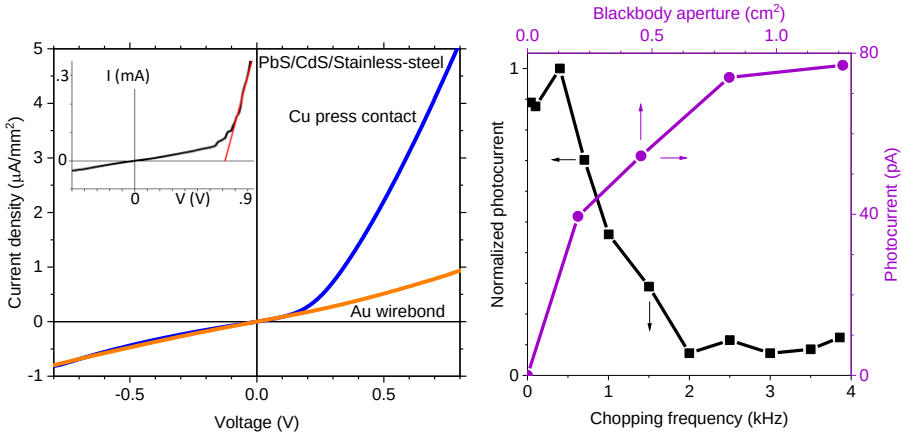

Figure 4. (left) Current density as a function of voltage for two electronic contacts. (Blue) j-V curve with copper press contact to PbS. (Orange) j-V curve with Au wire-bond contact. (inset) Current-voltage curve of a SPEED-grown CdS/PbS heterojunction solar cell [7]. (right, solid squares) Photo-current as a function of chopping frequency. (right, solid circles) Photo-current as a function of blackbody aperture area.

To confirm that strongly rectifying SPEED-grown PbS/CdS heterojunctions are possible, Figure 4 (left, inset) presents an unpublished I-V curve from our CdS/PbS heterojunction solar cell [7], where the ohmic contact to PbS was a 75-mm^2-area evaporated layer of gold. The contact to CdS was SPEED-deposited F-doped SnO_2 [19]. The maximum current density for the inset plot is about the same as in the main plot, but the threshold voltage is about 3x higher. The rectification ratio at ± 0.8 V is about 3. That device had a reported responsivity of 0.5 mA/W under 1 sun illumination [7], but it was not otherwise characterized as an infrared detector.

Figure 4 (right, solid squares) presents photo-current (before amplifier gain) as a function of chopping frequency. There is signal up to about 2000 Hz, which is fast compared to the expected response for any thermal effect.

Figure 4 (right, solid circles) presents photo-current as a function of blackbody aperture area. The curve is sublinear, so only the first point is used in the responsivity estimation. The radiance for a blackbody at 1100 ˚C in the 1-4 μm band is ~43,900 W/m^2-sr. The effective wire-bond contact area was taken to be 1.4 mm^2. The distance from aperture to detector was 30 mm, giving 0.0016 sr solid angle. The estimated responsivity is thus 30 nA/W. The measured current noise spectral density is 4.9 x 10^{-4} nA/(Hz)$^{1/2}$. The calculated detectivity is almost 10^4 cm·(Hz)$^{1/2}$/W (Jones).

DISCUSSION

Figure 2 shows a small curved barrier of height V_{bi} preventing hole flow from p-PbS to n^+-CdS, where the holes would recombine with electrons. Additionally, a small step barrier blocks minority-hole flow from n^+-CdS to PbS. From Eqs. (2, 3) we find Φ_B = 378 meV and V_{bi} = 213 mV.

When a positive bias is applied to the PbS top surface, it lowers the Fermi level there and drags down the PbS bands with it. This reduces the barrier to hole flow toward CdS and gives conditions for rapid current increase with bias, i.e. forward bias, in agreement with observations in Figure 4.

For negative bias applied to the PbS top surface, E_F increases on the left side, dragging the bands upward and increasing the barrier for hole flow from PbS to the junction, which constitutes reverse bias. The step barrier Φ_B for minority holes in CdS is unchanged by bias, which should result in a small constant reverse bias current, like for a standard metal-semiconductor Schottky junction [14]. However, our junction likely has leakage or unintentional photo-current due to ambient light, so the current increases with increasing reverse bias, though more slowly than for forward bias.

Our photoresponse measurements were performed without external bias. Under such conditions and according to Figure 2 (right), minority electrons photo-excited into the PbS conduction band can reduce energy by diffusing toward the interface, where no barrier blocks their crossing. This explains why we measure a photo-current.

Unlike a CdS-PbS solar cell, where CdS is the window layer, the IR absorption happens not at the interface, but on the opposite side of the PbS layer from the interface. Thus, high detector efficiency requires a suitable design that considers depletion width, absorption depth, and PbS layer thickness. To estimate the zero-bias depletion width from Eq. (4), we take $K_s \sim 100$, which is the value found at 5 kHz for nano-crystalline PbS films similar to our films [20]. We set the acceptor concentration N_A equal to the hole concentration $p = 1.2 \times 10^{15}$ cm^{-3} found from the Seebeck coefficient [12] using Eq. 1. We find $W = 1.4$ μm. The characteristic absorption depth in the 2-4 μm wavelength range is 0.2 μm, and our PbS films are about 0.5 μm thick [6]. Thus, we estimate that the depletion width is large enough for the built-in field to reach all the minority-carrier electrons excited in our PbS film.

One motivating factor for degenerately doping the CdS was the thought that no band-bending is required in CdS to collect the minority-carrier electrons excited in PbS. A second motivating factor was that, according to Figure 2 (right), a higher Fermi level in CdS would create suitable band-bending and built-in field in PbS to collect photo-excited minority-carrier electrons. If CdS were undoped, with a Fermi-level closer to mid-gap, its work function would exceed that of p-PbS. Then, the junction would be like an ohmic metal-semiconductor contact. This would disagree with the rectifying behavior we measured. Moreover, the PbS bands would be bent opposite to the way shown in Figure 2, which would disagree with our observation of a zero-bias photoresponse. The heavy doping of CdS, of course, needs to be balanced against the expected role of CdS as an electrical isolator between neighboring collection electrodes on the TFT. An additional undoped CdS isolation layer might be needed, along with consideration for its effect on the band-bending. To summarize the discussion of Figure 2 (right), the single assumption that SPEED-grown CdS has a work function as small as 3.47 eV, based on [11], allows us to qualitatively explain our observations.

We next discuss whether the metal contacts to the two sides of the heterostructure have any significant effect. Gold is known [21] to make ohmic contact with p-PbS, because gold's work function of 5.1 eV [22] exceeds the value ~3.6 eV for nearly intrinsic p-type PbS. We found no experimental report on copper-PbS junctions, but Cu's 4.65 eV [21] work function also exceeds that of p-PbS, so Cu should also form an ohmic contact.

As noted in Figure 4, the device with gold wire-bond contact was less rectifying than for the Cu press contact. Let us consider whether the Cu-PbS contact itself is rectifying. If a rectifying Schottky junction were formed, a negative bias on the Cu contact would raise the Fermi level in the metal relative to the PbS and lower the barrier to holes flowing in from the PbS [14]. In other words, for a Cu-PbS Schottky diode, negative bias on the contact would be forward bias. This is opposite to the sense of rectification in Figure 4.

We also consider the stainless steel contact with n-CdS. Though stainless steel's work function 4.3 eV [23] exceeds the value we have taken for CdS, which would be the condition for a rectifying metal-contact to a n-type semiconductor, we expect this junction

with degenerately-doped CdS to be more like a metal-metal junction with essentially no barrier to flow of electrons. Optically-excited minority-carrier electrons that make it from PbS to CdS would then freely flow into the substrate.

Thus, we estimate that the contacts have little effect on our measured IV curves or photoresponse. The difference in rectification may be caused by mechanical damage induced by ultrasonic wire-bonding of gold wire, which could cause shunts to ground that would reduce the rectification.

Prior work has demonstrated room temperature heterojunction n-CdS/p-PbSe photodiodes with responsivity of 55 mA/W and D* = 5 x 10^8 Jones at λ = 4.7 µm wavelength [8]. The earliest p-PbS/n-CdS heterojunction IR detector results we could find [9] claimed a D* of 1.5 x 10^{10} Jones at 3.3 µm. The values of these figures of merit exceed the values presented here. In [8], the PbSe was grown by molecular beam epitaxy (MBE) on silicon substrates, so the PbSe absorber layer would have had better crystal quality than the polycrystalline PbS layer we grew by aqueous heterogeneous reaction (SPEED). This would give better minority-carrier lifetime and diffusion length. In [9], PbS was chemically deposited on single crystal CdS, whose transport properties would have been superior to those for our CdS films. Nevertheless, the reports of high D* values for chalcogenide heterojunctions suggest that further investigation of spray deposited heterojunctions is justified due to the specified need for low cost detectors [1].

ACKNOWLEDGMENT AND DISCLOSURE

The work described in this paper was funded in part by Truventic and iCRco. Robert Peale and Isaiah Oladeji are owners of Truventic LLC and may benefit financially from the results presented here. Stephen Neushul is an officer and owner of iCRco and may benefit financially from the results presented here.

REFERENCES

1. U. S. Air Force Small Business Innovative Research Solicitation Topic AF193-005, “Readout Integrated Circuit for Low Cost Infrared Focal Plane Arrays” (2019).
2. Zeiss/Bosello X-ray imaging panel, Bosello High Technology USA LLC, 980 Executive Drive, Warsaw, IN 46580-8535 USA, bosello.eu.
3. Javaneh Bouromand and R. E. Peale, “Direct conversion X-ray detector array, Process design,” Final Report to iCRco, 31 October 2013, property of iCRco, Goleta CA, unpublished.
4. L. Dong, R. Yue, and L. Liu, “Fabrication and characterization of integrated uncooled infrared sensor arrays using a-Si thin-film transistors as active elements,” J. Microelectromechanical Systems. **14**, 5 (2005).
5. W. L. Wolfe and G. J. Zissis, editors, *The Infrared Handbook* (Office of Naval Research, Arlington VA 1978), Chapter 11.
6. H. Abouelkhair, P. N. Figueiredo, S. R. Calhoun, C. J. Fredricksen, I. O. Oladeji, E. M. Smith, J. W. Cleary, and R. E. Peale, “Ternary lead-chalcogenide room-temperature midwave infrared detectors grown by spray-deposition,” MRS Advances. **3**, 291 (2018).
7. Nagendra Dhakal, Seth Calhoun, Robert E. Peale, and Saiful Khondaker, “Spray-Deposited CdS/PbS Solar Cells,” Materials Research Society Fall Meeting 2018, Boston MA, abstract and poster presentation number ET11.12.26.

8. B. Weng, J. Qiu, L. Zhao, C. Chang, and Z. Shi, "CdS/PbSe heterojunction for high temperature mid-infrared photovoltaic detector applications," Appl. Phys. Lett. **104**, 121111 (2014).

9. S. Watanabe and Y. Mita, "Electrical Properties of CdS-PbS Heterojunctions," Solid-State Electronics. **15**, 5 (1972).

10. K. P. Bhandari, P. J. Roland, H. Mahabaduge, N. O. Haugen, C. R. Grice, S. Jeong, T. Dykstra, J. Gao, and R. J. Ellingson, "Thin film solar cells based on the heterojunction of colloidal PbS quantum dots with CdS," Solar Energy Materials & Solar Cells. **117**, 476 (2013).

11. D. H. Yeon, B. C. Mohanty, S. M. Lee, and Y. S. Cho, "Effect of band-aligned double absorber layers on photovoltaic characteristics of chemical bath deposited PbS/CdS thin film solar cells," Sci. Rep. **5**, 14353 (2015).

12. R. E. Peale, S. Calhoun, N. Dhakal, I. O. Oladeji, and F. J. González, "Spray-on thermoelectric energy harvester," MRS Advances. **4**, 851 (2019).

13. R. A. Smith, Semiconductors, 2nd ed. (Cambridge University, 1978).

14. R. F. Pierret, *Semiconductor device fundamentals* (Addison-Wesley, Reading, 1996), pp. 477-501.

15. R. L. Anderson, "Germanium-Gallium Arsenide Heterojunctions, Lett," IBM J. Res. Dev. **4**, 3 (1960).

16. N. B. Kindig and W. E. Spicer, "Band Structure of Cadmium Sulfide—Photoemission Studies," Phys. Rev. **138**, A561 (1965).

17. R. M. Oman and M. J. Priolo, "Photoelectric Properties of Lead Sulfide near the Threshold Region," J. Appl. Phys. **37**, 524 (1966).

18. H. Khallaf, G. Chai, O. Lupan, L. Chow, S Park, and A. Schulte, "Investigation of aluminium and indium in situ doping of chemical bath deposited CdS thin films," J. Phys. D: Appl. Phys. **41**, 185304 (2008).

19. R. E. Peale, E. Smith, H. Abouelkhair, I. O. Oladeji, S. Vangala, T. Cooper, G. Grzybowski, F. Khalilzadeh-Rezaie, and J. W. Cleary, "Electrodynamic properties of aqueous spray deposited SnO_2:F films for infrared plasmonics," Opt. Eng. **56**, 037109 (2017).

20. S. Sagadevan and A. S. Sundaram, "Dielectric properties of lead sulphide thin films for solar cell applications," Chalcogenide Lett. **11**, 159 (2014).

21. D. B. Strasfeld, A. Dorn, D. D. Wanger, and M. G. Bawendi, "Imaging Schottky Barriers and Ohmic Contacts in PbS Quantum Dot Devices," Nano Lett. **12**, 569 (2012).

22. Timothy J. Drummond, "Work Functions of the Transition Metals and Metal Silicides, Sandia National Laboratories," Report Number SAND99-0391J (1999).

23. R. G. Wilson, "Vacuum Thermionic Work Functions of Polycrystalline Be, Ti, Cr, Fe, Ni, Cu, Pt, and Type 304 Stainless Steel," J. Appl. Phys. **37**, 2261 (1966).